



Numerical Study and Theoretical Comparison of Outlet Hole Geometry for a Gravitational Vortex Turbine

Alejandro Ruiz Sánchez¹, Jorge Andrés Sierra Del Rio^{1,2}, Toni Pujol³

¹Department of Mechatronics Engineering, MATyER, Instituto Tecnológico Metropolitano, 050034, Medellín, Colombia.

²Department of Mechanical, GIAM, Institución Universitaria Pascual Bravo, 050054, Medellín, Colombia.

³Area de Mecànica de Fluids, Departament d'Enginyeria Mecànica i de la Construcció Industrial, Universitat de Girona, Campus Montivili, 17071, Girona, Spain.

Correspondence: E-mail: alejandraruiz190787@correo.itm.edu.co

ABSTRACT

The gravitational water vortex turbine is an alternative to renewable energies, it transforms the hydrokinetic energy of the rivers into electric energy and it does not require a reservoir. According to studies carried out, the hydraulic efficiency can increase or decrease according to the turbine geometrical configuration. This paper presents a numerical (CFD) and analytical comparison between conical and cylindrical designs for the outlet. The results show a higher performance for conical geometry than the cylindrical tank. The fluid behavior in CFD and analytical studies presents a tangential velocity increase near to air core and outlet hole (similar behavior). The maximum theoretical power generated was 167 W and 150 W for conical and cylindrical design respectively. The differences between geometries of the outlet holes using CFD and analytical models were 11 and 7%, respectively. However, the closest results to the CFD model had different values of 31 and 29% for conical and cylindrical design, respectively. The furthest result regarding the CFD study was 55%. The principal difference is due to tank geometry, the change in discharge zone, as well as the ratio of diameter tank and outlet hole can increase or decrease the tangential velocity and make a stronger and more stable vortex formation. The theoretical power generated is a good parameter to select the height to place the rotor.

ARTICLE INFO

Article History:

Submitted/Received 05 Oct 2020

First revised 29 Des 2020

Accepted 02 Mar 2021

First available online 18 Sep 2021

Publication date 01 Dec 2021

Keyword:

Geometry,
Power plan,
Renewable energy,
Tank,
Vortex.

1. INTRODUCTION

According to the United Nations conference, access to electricity guarantees sustainable development for rural communities. The main disadvantage of rural communities is the difficult access and that is far from the national interconnected system, these communities are known as non-interconnected zones (NIZ). The NIZ need a decentralized generation system to increase their quality of life (Márquez et al., 2010; Rehan & Pao, 2019). Small Hydropower Plants (SHP) have shown greater implementation in these areas due to their low installation cost, easy construction, and low carbon dioxide emissions (Date & Akbarzadeh, 2009; Mohamed, 2018). However, the main problem with SHP is low efficiency around 90% (Dhakal et al., 2018). The gravitational vortex turbine (GVT) is an alternative to SHP, does not require a complex design for fabrication, and has no

water dam. Some of the main advantages of the GVT are the oxygenation of the water due to the interaction of water and air at the vortex interface, and the free circulation of fish through it due to its low revolutions (Rahman et al., 2017).

The operating range of the GVT is due in part to the fluid (head and flow) and on the other hand to the design of the tank and rotor. Figure 1 presents the operating range of the GVT concerning other turbines of greater and equal electric generation due to the height and flow.

The GVT is shown in Figure 2. The open rectangular channel stabilizes the flow derived from a river. Then, the flow is accelerated by a contraction before entering the tank. The flow enters tangentially to the circular tank, but due to the high level between the inlet and outlet, a gravitational vortex is formed. The forces in this vortex are the gravitation and the Coriolis. The water path line is a spiral around the outlet axis.

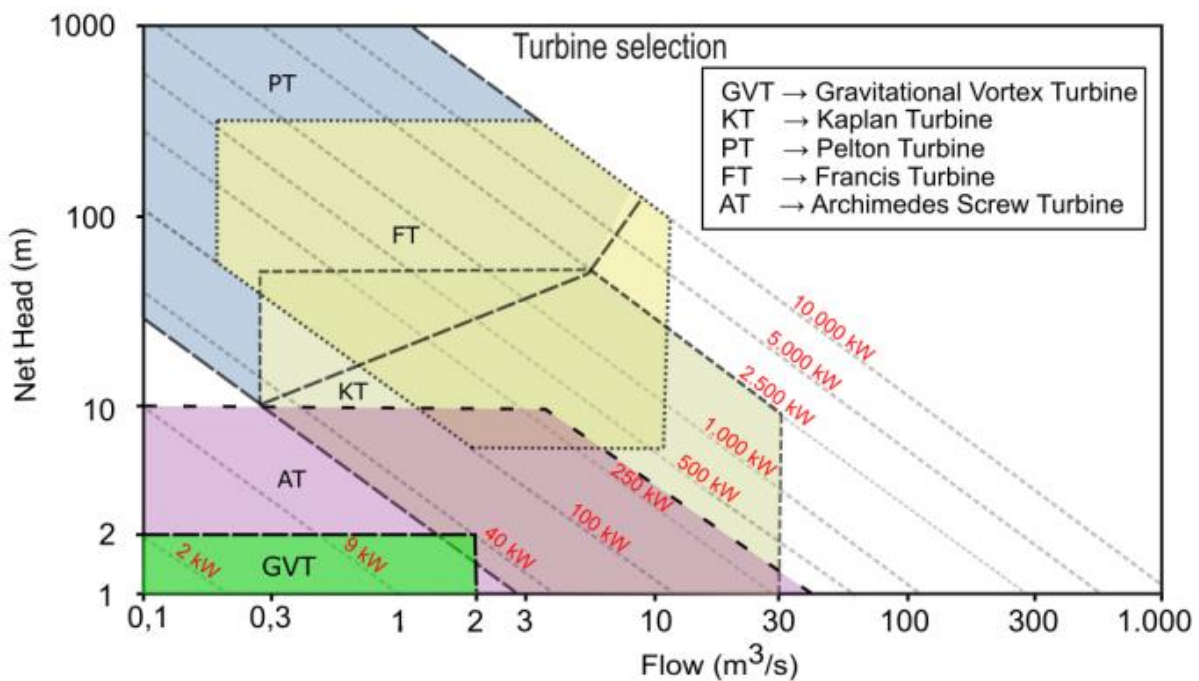


Figure 1. Operation range of GVT and other power plants.

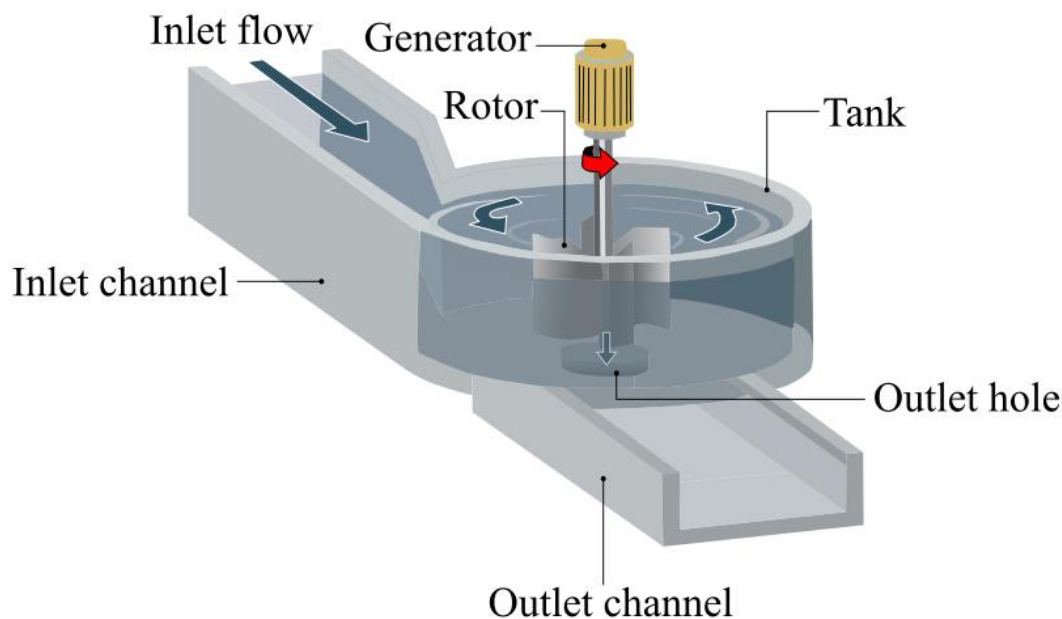


Figure 2. GVT parts and configuration.

2. PREVIOUS STUDIES

2.1. Analytical Studies

There is not a standard model to characterize the vortex to correlate the geometrical variables and the power generated by the GVT. From left to right **Table 1** presents authors and references, their mathematical correlations to characterize the free surface-induced vortex, and some comments. v_θ and v_z are the tangential and axial velocity respectively, Γ is the circulation, r is the water radius, r_c is the air core radius, ν is the kinetic viscosity, c is the constants, g is the gravity acceleration, and H is the vortex height. The equation can be written in Equation [1] and [2]:

$$\Gamma = \oint_L \vec{v} dL \tag{1}$$

where \vec{v} is the velocity field and L is the vertical axis at the surface. However, Stoke's theorem express the previous equation with velocity field rotational.

$$\Gamma = \iint_A (\nabla_x \vec{v}) \cdot dA \tag{2}$$

where A is the surface area. The velocity field rotational ($\nabla_x \vec{v}$) is equal to vector field vorticity (Ω), the Equation [3] is expressed as:

$$\Gamma = \iint_A \Omega dA \tag{3}$$

Figure 3 shows the front and top view of GVT explaining the variables mentioned in **Table 1** in a water particle (wp) inside the turbine.

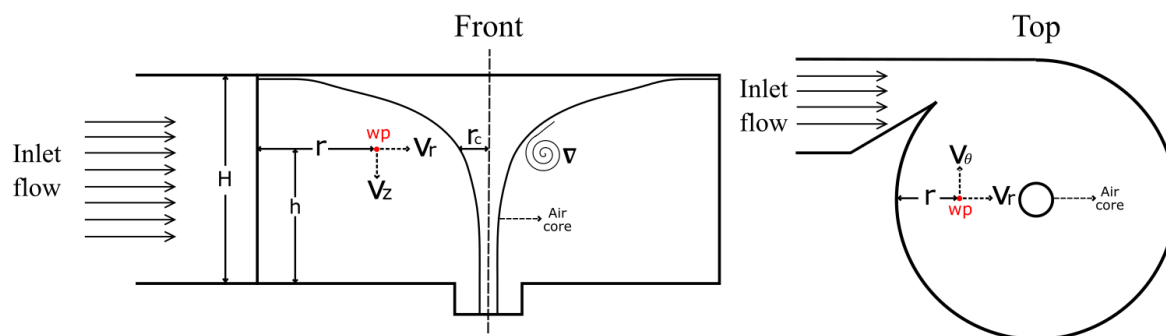


Figure 3. Velocity profiles and variables for water particles inside GVT.

Table 1. Mathematical models to characterize the vortex.

Author	Tangential velocity equation	Comments
(Mulligan et al., 2014)	$v_{\theta}(r) \propto 1/r$	-
	$v_{\theta}(r) = \frac{\Gamma}{2\pi r}$	-
(Einstein & Li, 2011)	$v_{\theta}(r) = \frac{\Gamma}{2\pi} \left(\frac{r}{(r_c^4 + r^4)^{\frac{1}{2}}} \right)$	when $0 \leq r \leq \infty$
	$v_{\theta}(r) = \frac{\Gamma}{2\pi} \left(\frac{r}{(r_c^2 + r^2)} \right)$	-
(Vatistas et al., 1986)	$v_{\theta}(r) = \frac{\Gamma}{2\pi} \left(\frac{2r}{(r_c^2 + 2r^2)} \right)$	-
	$v_{\theta}(r) = \frac{\Gamma}{2\pi r} [1 - \exp(-\frac{1}{4} \frac{v_z}{Hv} r^2)]$	-
(Rosenhead, 1930)	$v_{\theta}(r) = \omega r = \frac{\Gamma}{2\pi} \frac{r}{r_c^2}$	when $r < r_c$
	$v_{\theta}(r) = \frac{\Gamma}{2\pi r} = \omega \frac{r_c^2}{r}$	when $r > r_c$
(Hite Jr & Mih, 1994)	$v_{\theta}(r) = \frac{AC}{2\pi r} (e^{-\frac{Ar^2}{2\pi}})$	-
	$v_{\theta}(r) = \frac{(\Gamma_{\infty})(r_c)}{\sqrt{[8(r_c^2)(g)(\pi^2)(H-h) + \Gamma_{\infty}^2]}}$	-
(Odgaard, 1986)	$v_{\theta}(r) = \frac{\Gamma d \sqrt{2(g)(H+h)}}{2(\pi)(r)}$	-

2.2. Numerical Studies

Coriolis force is the most predominant factor in the vortex formation and acceleration is generated by Coriolis force. Wanchat & Suntivarakorn, (2012) established the tangential velocity are directly proportional to the water height within the tank. Wanchat et al., (2013) found that outlet diameter is between 14% and 18% of tank diameter to obtain the highest power generation. Şibil et al., (2021) obtained with the BSL RSM turbulence model the nearest results according to experimental and analytics results. Marian et al., (2012) concluded the tangential velocity increases from the walls and the maximum values are close to the vortex nucleus. Dhakal et al., (2014) determined the highest outlet velocity was obtained with a tank conicity of 23° and an angle of the channel of 43°. Shabara et al., (2015) performed a numerical study in ANSYS Fluent with experimental measurements, the authors reported a difference of 2 and 7% between the numerical and experimental

errors to prove the validity of the numerical model. Wichian and Suntivarakorn, (2016) studied the effect of the number of blades and the width of the blades. The experimental results at 0.06 m³/s showed that the turbine with 50% in width produced the highest torque and higher efficiency concerning the 0% in width (Wichian & Suntivarakorn, 2016). Dhakal et al., (2018) performed a numerical and experimental analysis to evaluate three different rotors formed by straight, twisted, and curved profiles. The results showed that the curved profile is the most efficient (82%) compared to straight blade (46%), and twisted blade (63%) (Dhakal et al., 2018). Although there are different numerical and experimental studies to improve the efficiency of GVT from modifications in its geometric configuration. The study of the outlet hole geometry effect is a parameter of great potential for improvement in efficiency hydraulics of the GVT because directly affects the vortex formation, specifically on its tangential

velocity and therefore on fluid outlet velocity from the tank.

Therefore, this work highlights the importance of proposing a new geometrical outlet configuration of the GVT. This study aims to evaluate the outlet velocity in two chambers with different outlet geometry: conical and cylindrical design by CFD.

3. METHODS

3.1. Governing Equations

Both fluids (air and water) are sharing the same velocity fields and turbulence. The governing equations for the unsteady, viscous, and vortex formation turbulent flow are continuity and Navier Stokes described (Laaraba & Khechekhouche, 2018) in Equation [4] and [5] respectively:

$$\frac{\partial v_r}{\partial r} + \frac{\partial v_z}{\partial z} + \frac{v_r}{r} = 0 \quad (4)$$

$$\frac{\partial \bar{u}}{\partial t} + \bar{u} \cdot (\nabla \bar{u}) = -\frac{1}{\rho} \nabla p + \nu \nabla^2 \bar{u} + \bar{g} \quad (5)$$

where g , ν and ρ are gravitational acceleration, viscosity, and density respectively. \bar{u} represents velocity vector

and it is defined in Equation [6] and ∇ reduces the partial derivation in each component (x, y, z) and it is explained by Equation [7].

$$\bar{u} = (u, y, w) \quad (6)$$

$$\nabla = \frac{\partial}{\partial x}, \frac{\partial}{\partial y}, \frac{\partial}{\partial z} \quad (7)$$

3.2. Geometry

As shown in **Figure 2** the GVT chamber can be divided into two main parts: the inlet channel (with length, width, and height of the inlet channel and area reduction) and the tank (with parameters such as tank diameter, outlet diameter, and outlet channel). Inlet channel height and area reduction parameters were selected as suggested by (Dhakal *et al.*, 2014) and the ratio tank diameter and outlet diameter were selected from outlet cylindrical was configured according to (Shabara *et al.*, 2015). **Figure 4a** shows the input channel dimensions used for each turbine design. **Figure 4b** and **4c** show the design and geometry dimensions of each turbine studied. The GVT was modeled in ANSYS® *SpaceClaim* software V19.2.

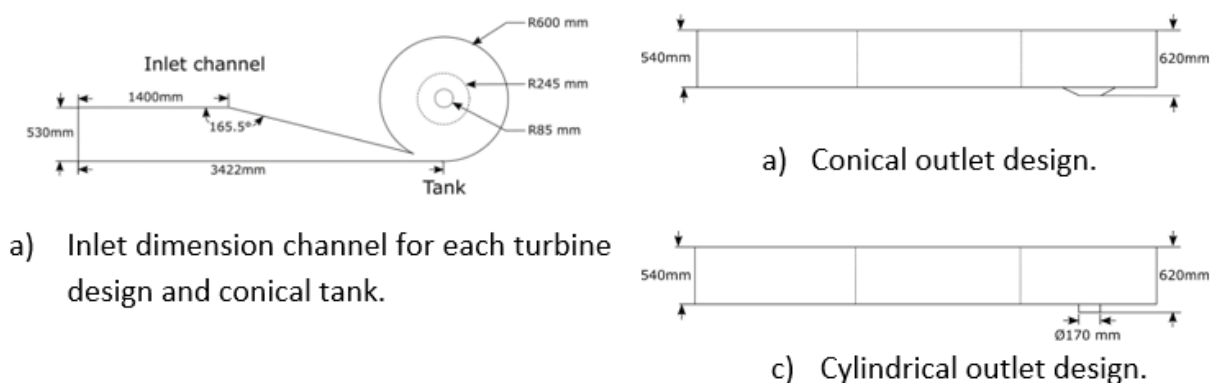


Figure 4. GVT inlet channel, conical and cylindrical dimension (millimeters).

3.3. Discretization Process and Boundary Conditions

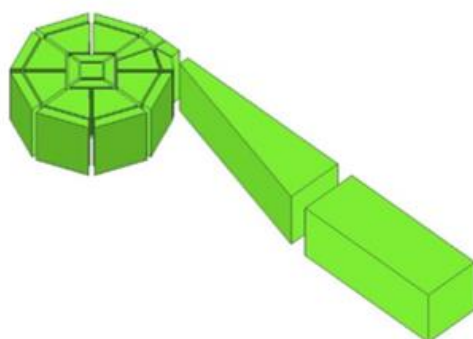
The discretization of the control volume was carried out in the "ICEM" module by ANSYS® software V19.2. The mesh is composed of 38 blocks unstructured to obtain $[1.1 \times 10]^5$ and $[1.2 \times 10]^5$ hexahedral elements for conical and cylindrical design respectively. The elements inside the GVT correspond to the fluid inside the tank, as shown in **Figure 5a**. The mesh was made in this module because it obtains high metrics in mesh quality and reduces the computational time (Du et al., 2018). **Table 2** shows the mesh metrics for conical and cylindrical outlet designs. Validation of configured meshes is performed by ensuring that the most important mesh metrics in CFX are in the acceptable range. The mesh Independence was obtained with 4 (four) meshes configuration keeping the metrics for all cases, to guarantee a difference in results of the convergence criterion less than 3% (Rehan & Pao, 2019). Two convergence

criteria were defined: water velocity in a point with coordinates $[-0.15; 0; 0.05]$ m (the coordinate axis aligned with tank axis and located at the tank bottom) and circulation in a surface with a radius of 0.15 m and height of 0.05 m as shown in Equation [1].

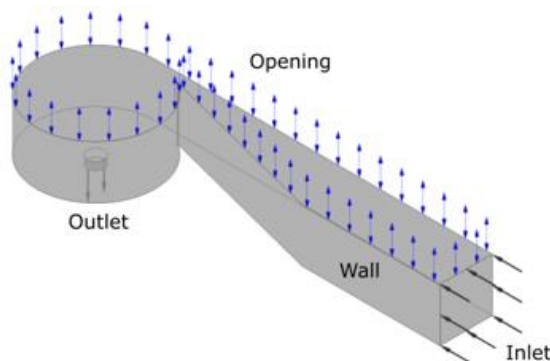
Figure 5b outlines the boundary conditions associated with the control volume. They are established according to the operating conditions of the turbine, in the following manner: the inlet velocity of 0.3 m/s (85 l/s) is associated with the flow rate and rectangular area of the inlet channel. The upper part of the GVT is configured as an Opening of (0 Pa) manometric pressure, which enables the fluids to enter and exit the control volume. The outlet hole was configured as an Outlet open to the atmosphere (0 Pa) (Rehan & Pao, 2019). The walls were assumed to be non-sliding as a representation of the GVT's surfaces. The system is governed by a subsonic flow ($Ma < 1$) and a relative pressure of zero Pascals (0 Pa).

Table 2. Mesh metric for conical and cylindrical outlet design.

Turbine	Element Size (mm)	Max Aspect ratio	Minimum Quality	Determinant 3x3x3
Conical	35	7.36	0.392	0.392
Cylindrical	35	18.20	0.572	0.710



a) Multi-blocks ICEM CFD.



b) Mesh Independence for each GVT design

Figure 5. Mesh independence for conical and cylindrical outlet design.

Water and air were selected as study fluids, both at 25°C to ensure that there is no change in the properties of any fluid, with a surface tension coefficient of 0.072 $[(\text{Nm})^{-1}]$. According to Şibil *et al.*, (2021) the turbulence model selected was Baseline Reynolds Stress Model (BSL RMS). It predicts vortex behavior in a circular tank. It is due to a comparison of the results between the numerical, experimental, and analytical models proposed by Vatistas *et al.*, (1986).

The simulation was run in a transient stage with a total time of 30 s at an adaptive time step which varies between $[1 \times 10]^{-3}$ and $[1 \times 10]^{-4}$ s, where the maximum time step was calculated with Equation [8] to ensure a Courant number less than 1. In addition, $[1 \times 10]^{-4}$ was selected as the convergence criterion for the residues obtained by Root Mean Square (RMS).

$$C = \frac{V * \Delta t}{\Delta x} \quad (8)$$

where C is the dimensionless Courant number, V is the magnitude of the velocity, Δx the minimum mesh size, and Δt the time step.

Figure 6 shows the mesh independence for both designs. the simulation started with 1.9×10^4 and 2.2×10^4 elements for conical and cylindrical design respectively and was running at 2.5×10^5 y 2.6×10^5 elements for conical and cylindrical design respectively. the outlet velocity and circulation for conical design were 1.5 and 2.1 m/s respectively and for cylindrical was 1.2 and 1.9 m/s respectively.

4. RESULTS AND DISCUSSION

4.1. CFD Results

Figure 7 shows the planes where the velocity contour, volumetric fraction, vectors, and tangential velocity profiles are shown at the vertical plane (XY) and horizontal plane (XZ).

The figure also exemplifies the reference height for the planes that will be used to determine the velocity profiles. The coordinate axis that was taken as a reference for this study is also shown in the figure, where gravity was taken in the negative Y-axis.

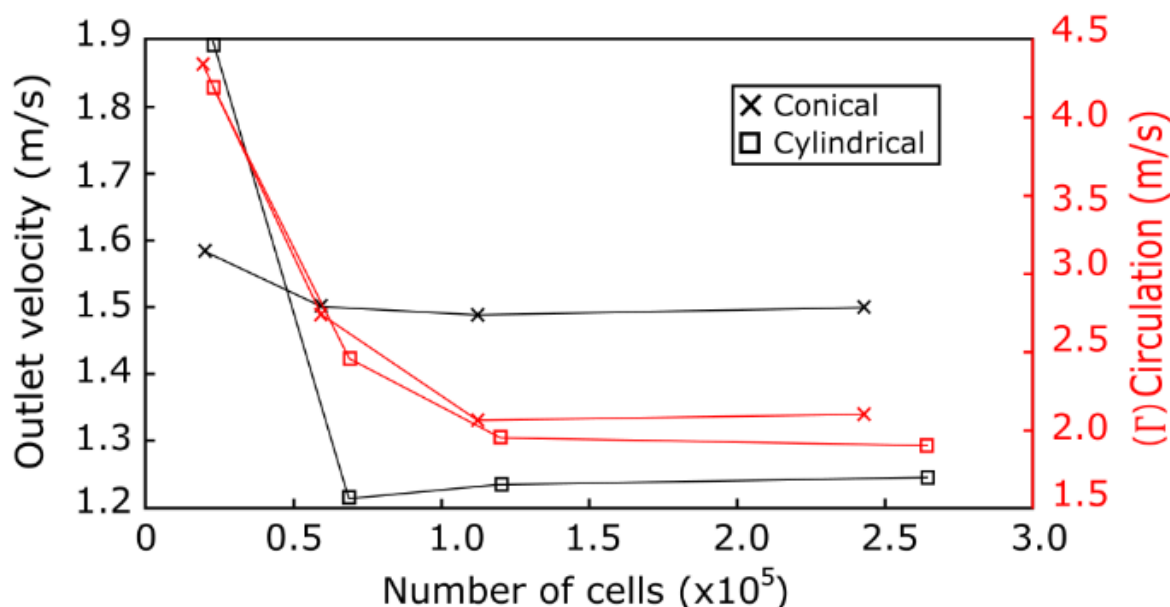


Figure 6. Operating conditions for both conical and cylindrical outlet design.

Figure 8a and 8b (left) present velocity streamlines for each geometry, while Figure 8a and 8b (right) show the vortex core isosurface with a water volume fraction 0 (zero) for both geometries. The streamlines show the inlet channel manages to stabilize the flow and as it accelerates when reaching the area reduction and enters the tank tangentially to have a faster vortex formation. The isosurface shows the air core completely formed in both tanks, it indicates

the geometries are suitable for harnessing the kinetic energy of the fluid. The volume control settings correctly represent the behavior of the hydraulic system, highlighting the inlet flow as the main configuration parameter. A low water inlet does not allow the formation of the vortex, and an abundant flow causes flooding in the tank, which eventually deforms and affects the vortex performance.

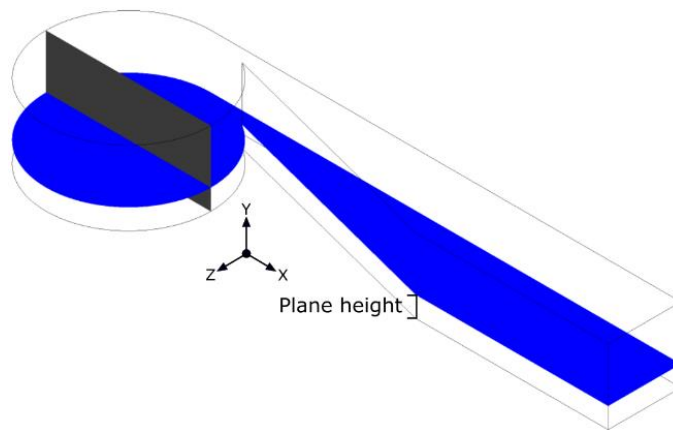
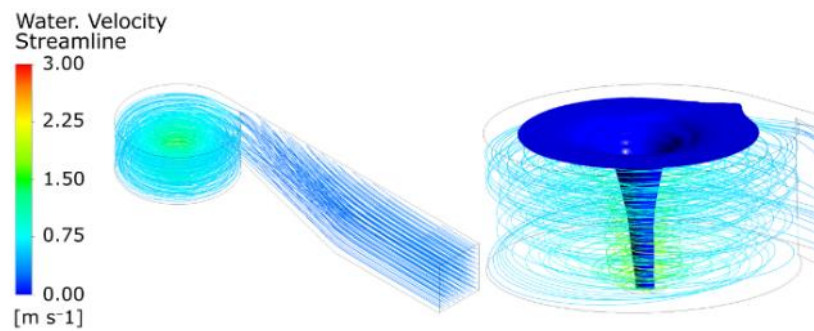
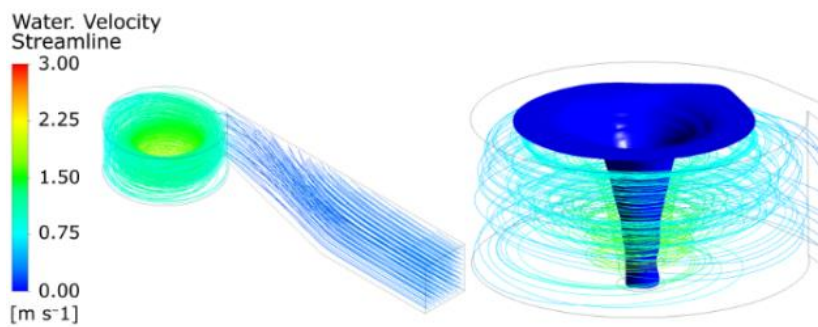


Figure 7. Results vertical and horizontal display planes.



a) Conical outlet design



b) Cylindrical outlet design

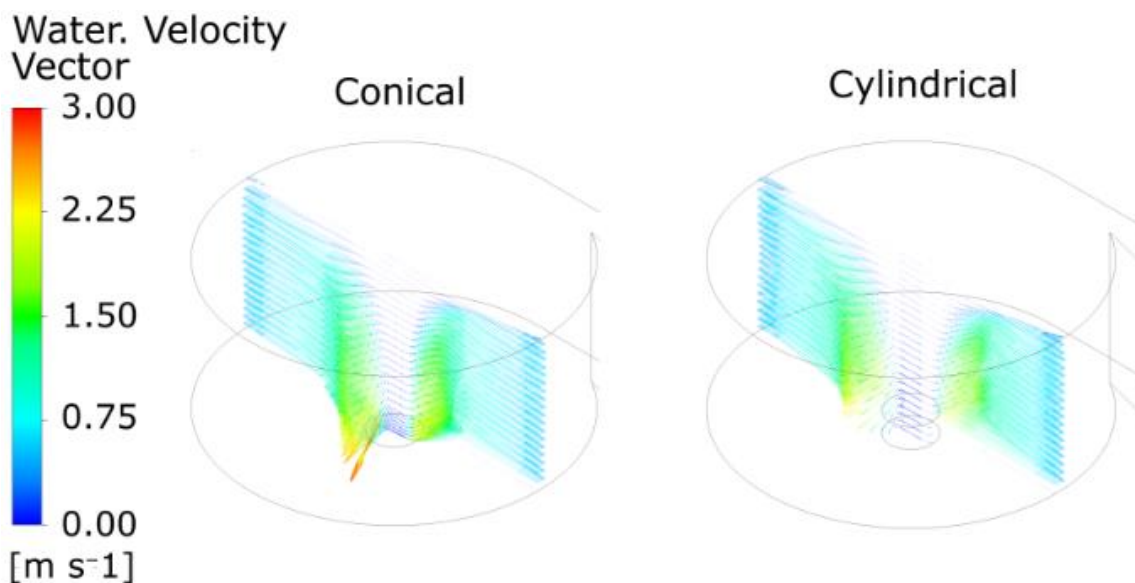
Figure 8. Velocity streamlines for both conical and cylindrical outlet design.

Figure 9a represents velocity vectors in both geometries, where it is shown that the fluid in the conical section tank (left) gains higher outlet velocity than the cylindrical section tank (right). Additionally, the fluid vectors in the walls are 0 m/s and increase as it approaches and descends through the air core.

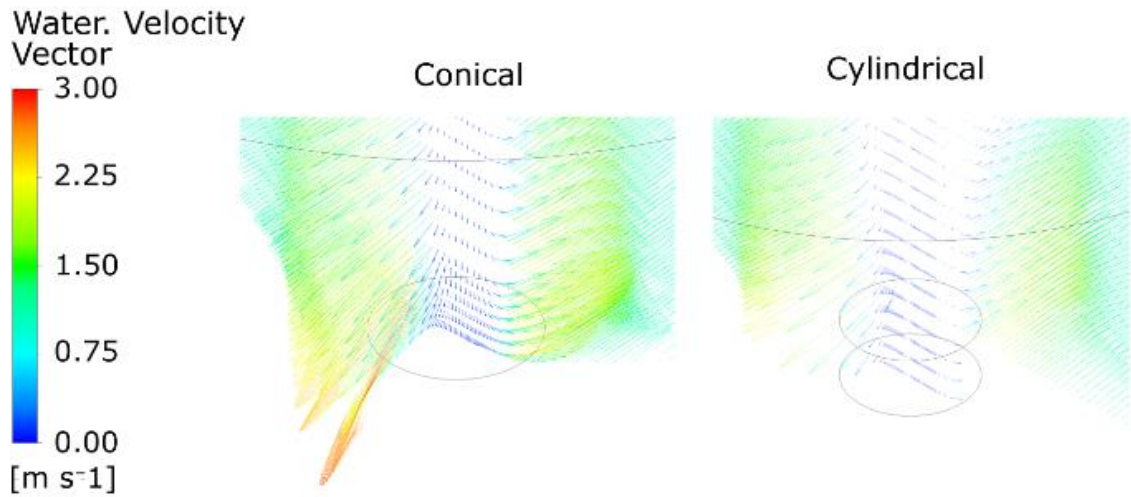
Figure 9b shows an approach to the discharge zone of each of the designs. This figure helps to exemplify vectors in the discharge zones. It is observed that the magnitude of the vector in the conical geometry is greater than cylindrical geometry, where the difference is observed in the final part of the tank.

Figure 9c and **9d** represent the velocity gradient vectors on the Y coordinate axis (it should be noted that gravity for this study was taken on the Y-axis) for the conical and cylindrical design respectively. This figure represents the fluid velocity increase as it

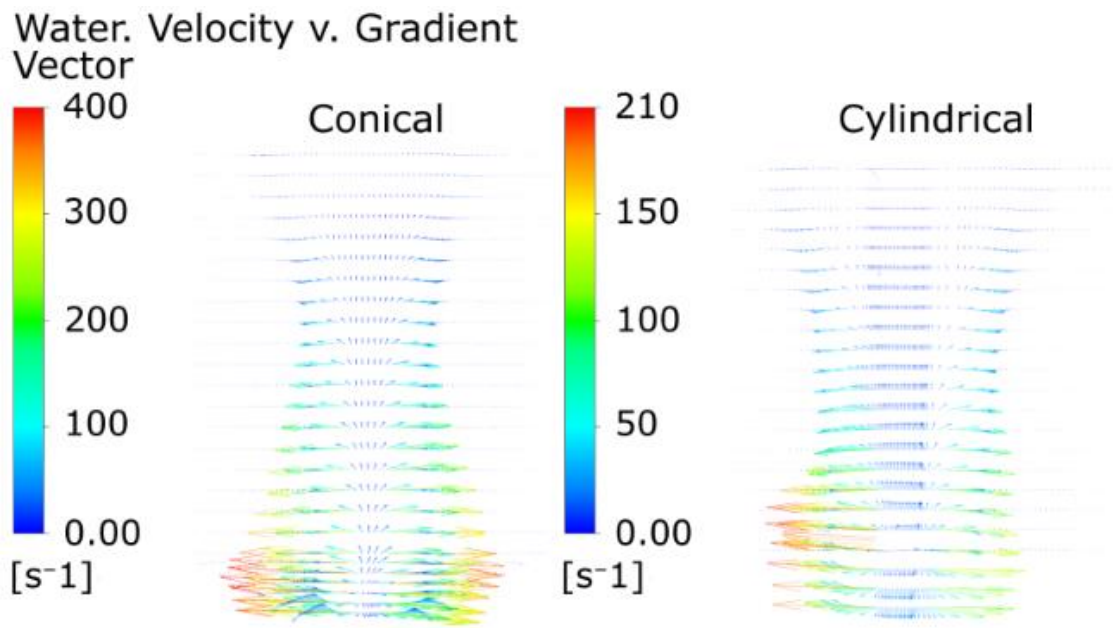
descends through the tank and reaches the outlet hole. On the other hand, in both figures it is observed that velocity increases considerably in the discharge zone for each design, this corroborates the above mentioned where it is mentioned that fluid velocity increases as it approaches the nucleus and descends by it. Similarly, the difference between the two geometries is observed in the discharge zone, in which the fluid in the conical geometry presents the upper gradients symmetrically and increasing to the tank outlet. For cylindrical geometry, fluid velocity gradients are presented equally to the conical in the discharge zone. However, for this geometry the change in speed in height is not as considerable as in conical geometry. In addition, gradients are presented on the left side of the vortex, meaning that the vortex is being affected.



a. Water velocity vectors for each design.



b. Water velocity vectors for each design (Zoom).



c. Water velocity v. Gradient vectors for each design.

Figure 9. Water velocity vectors and water velocity v. Gradient vectors for each design.

Figure 10 represents the change in numerical tangential velocity of the fluid as it approaches the center of the chamber, the velocity is taken in a horizontal plane of the chamber at 3 different heights (50, 100, and 200 mm) measured from the bottom of the tank. Numerical results show an increase in tangential velocity as it approaches the tank center, it is because the fluid circulation radius is lower, but the rotating velocity increases significantly. The tangential velocity profile of both designs has the same behavior, the highest velocity between the planes is at the closest to the bottom (50

mm) with values of 1.9 and 1.7 m/s for the conical and cylindrical design, respectively. Between two geometries there is an 11% difference in tangential velocity in the lowest height plane. Similarly, the graph shows that the conical geometry has a higher velocity at the three different heights, with a difference of 10% for the other heights. However, it is also noted that in the radius between 0.2 and 0.6 m the velocity is the same for each design. From 0.2 m, it is observed the greatest increase in speed to reach its highest point. The change between 0.1 and 0.2 m

radius is 39% and 40% for the conical and cylindrical design, respectively.

However, the highest tangential velocity achieved in both geometries is presented at the bottom of the discharge section with 2.1 m/s and 1.9 m/s for the conical and cylindrical design respectively. The tangential velocity was calculated using Equation [9], where the velocity coordinates vectors were obtained by Ansys.

$$V_{\theta}(r) = V_x \sin \beta - V_z \cos \beta$$

According to **Figure 7**, there is no β angle between X and Z positions. Therefore, $V_{\theta}(r)$ was calculated by the next equation:

$$V_{\theta}(r) = -V_z \quad (9)$$

Figure 11 shows the water velocity contour for each geometry. In addition, an approach is shown in the discharge zone for each geometry showing the velocity vectors above the boundary. Both geometries show a stable and symmetrical vortex formation, and both cases exemplify the above where the fluid increases its velocity as it approaches the air core and outlet hole, even the zero velocity on the walls. The behavior is identified better in the discharge zone, where the magnitude of the velocity vector increases significantly by a short distance

(height of the discharge zones). However, the geometries have a higher percentage of water on the left side of the discharge section and are a result of fluid area reduction inlet to the tank. On the other hand, the conical geometry shows a higher average fluid velocity in the tank with 0.71 m/s and cylindrical geometry of 0.67 m/s, the difference is because the cylindrical geometry has a greater loss in the walls. The behavior is due to discharge sections, where the first case has a soft discharge section (153°) and in the second case the change is more abrupt (90°).

Figure 12 shows a water volume fraction contour for each geometry, where 100% and 0% water are represented by red and blue respectively. Both geometries observe the interaction between the two fluids in the air core vortex. Both designs have a symmetrically and steadily vortex formation. However, in the discharge section, the conical geometry (left) has a higher percentage of water in the discharge section concerning the cylindrical geometry (right). It is due to the change in the discharge zone, the cylindrical part being an abrupt change generate higher turbulence, and fluid begins to recirculate in this section, which results in losses in hydraulic efficiency (see bottom tank geometry **Figure 11**)

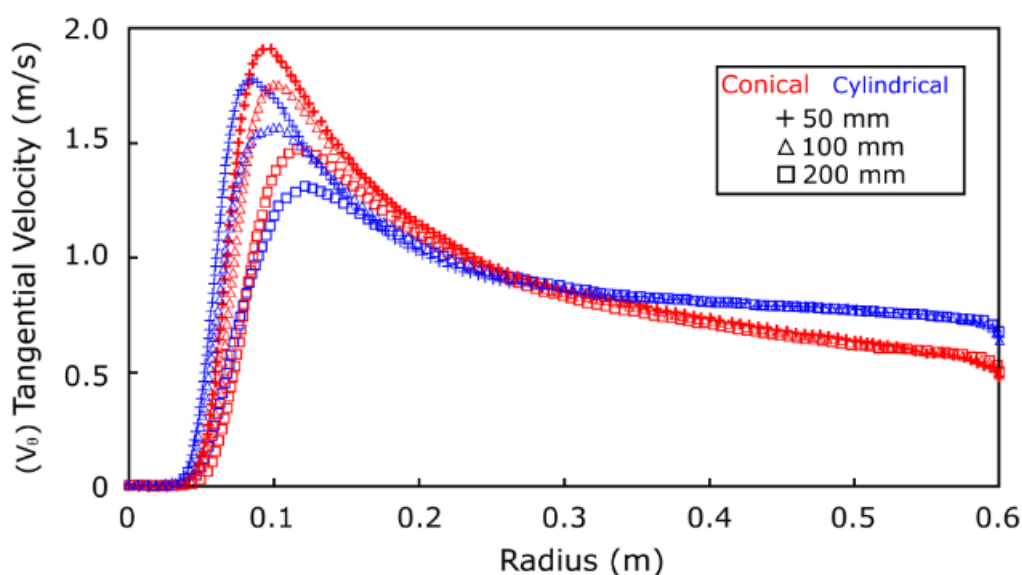


Figure 10. Numerical water velocity at different heights horizontal planes for $h = 50, 100,$ and 200 mm.

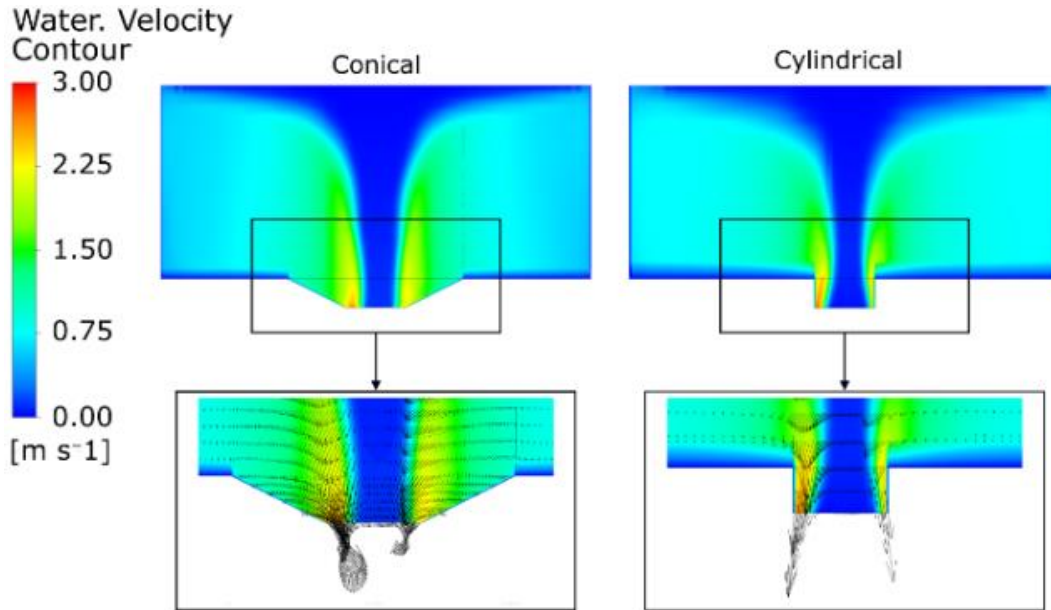


Figure 11. Water velocity contour for each geometry.

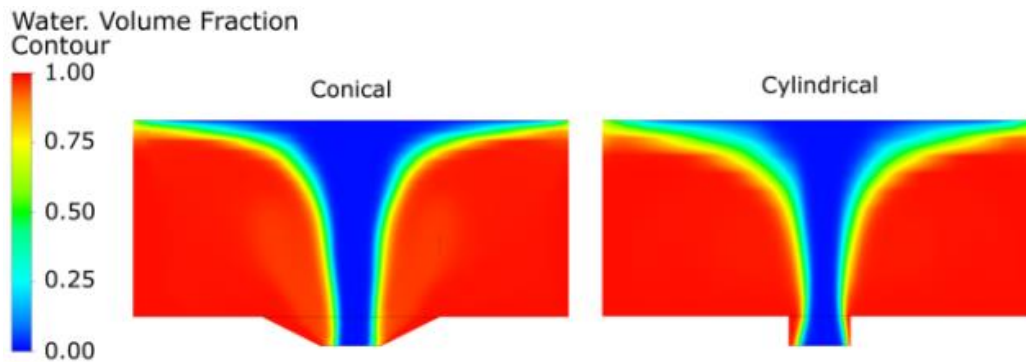


Figure 12. Water volume fraction contour.

To determine a theoretical mechanical power to the turbine height, a 9 mm³ water cube was determined and the highest tangential velocity will be taken on each plane (used to calculate the velocity profiles) as the reference velocity. **Table 3** shows the theoretical power generated by each outlet hole geometry. The conical geometry has a higher power generated compared to the cylindrical design, this shows a 9% error for each power at different heights. In addition,

it is shown that the highest power generated is the same at the height of 50 mm, it has a higher tangential velocity compared to the other heights. In this way, the height at which the rotor must be placed to extract greater kinetic energy from the fluid and transform it into mechanical energy. It should be noted that the rotor diameter should also be considered for the location of the rotor because the rotor can interact with greater fluid speed while it is closer to the core.

Table 3. Theoretical power generation for each design in different heights.

Geometry	Conical			Cylindrical		
Height (mm)	50	100	200	50	100	200
Power (W)	167	154	130	150	141	115

4.2. Numerical vs Analytical Models

By reviewing the literature, it was determined that the numerical results delivered by ANSYS were compared with the models proposed by Einstein & Li, (2011), Vatistas *et al.*, (1986), Rosenhead, (1930), and Hite Jr & Mih, (1994) (Table 1). They were compared to each other and with the results of an experimental test in previous research (Mulligan *et al.*, 2019). In addition, these models have a higher level of detail in their variables compared to unused studies. Figure 13 shows the comparison between the tangential velocity of CFD and analytical models mentioned for each geometry design at a height of 5mm from the camera background (by showing higher tangential velocity in both geometries in the CFD results). The figure shows analytical models represent the fluid behavior in a way to CFD study. In addition, a highest velocity close to the air core (approximately 0.1 m radius) and a lowest fluid velocity in the walls (radio 0.6 m) and air core are observed. The analytical models and the CFD study show the geometry with the highest tangential velocity

is conical. It should be noted that the mathematical models were calculated with the circulation obtained in the CFD study to determine the same conditions in all studies.

However, Figure 13 also shows a large difference between the CFD model and the analytical model. From left to right Table 4 represents the models compared to the velocity profiles obtained from the CFD study, the value of the highest velocity in the conical and cylindrical geometry, the relative error between geometries for each model, and the relative error of the values of each proposed model concerning the CFD study for conical and cylindrical geometry. The error between geometries in each analytical model is approximately 8%, while the difference in models in the CFD study is 11% as mentioned above. The model that differs least from the CFD study corresponds to proposed by Einstein & Li, (2011). With an error of 31 and 29% for conical and cylindrical geometry respectively. The model proposed by Rosenhead, (1930) presents the most error concerning the CFD study. With a difference of 55 and 53% for conical and cylindrical geometry respectively

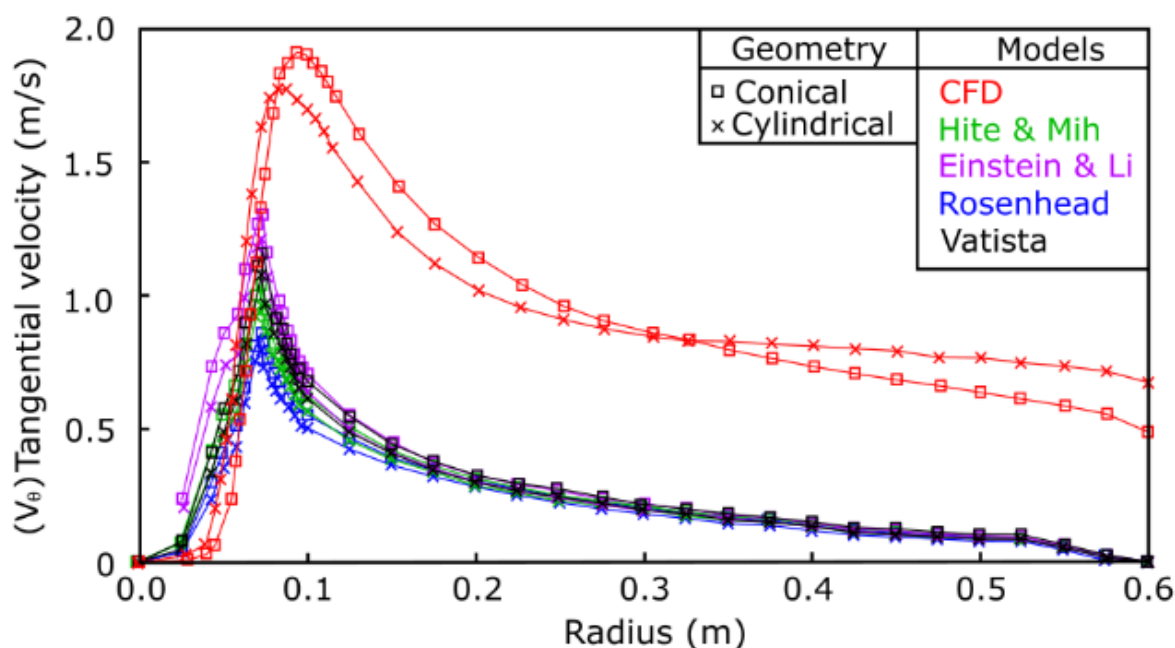


Figure 13. Numerical and analytical comparison for each design at h=50 mm.

Table 4. Tangential velocity and difference in numerical and analytical studies.

Study	Vel. Conical (m/s)	Vel. Cylindrical (m/s)	Geometry difference (%)	Conical difference (%)	Cylindrical difference (%)
CFD	1.91	1.70	11	0	0
(Einstein & Li, 2011)	1.31	1.21	8	31	29
	1.16	1.07	8	39	37
(Vatistas et al., 1986)	0.86	0.82	7	55	53
	1.04	0.96	8	45	44

The difference between the models and the CFD study is mainly attributed to the geometry used. For example, the model proposed by Vatistas et al., (1986) studied the vortex formation in a cylindrical tank with a difference in height between the inlet channel and the bottom of the tank. Unlike this study, the inlet channel is at the same level as the camera background. The difference in geometry allows increasing the error between the two models, mainly in the fluid inlet to the tank which affects the vortex on one side. Otherwise, the aspect ratio between the diameter of the tank and the diameter of the outlet hole determines the diameter of the air vortex formed in the tank (Wanchat et al., 2013). However, the results of this study are similar to the study conducted by Mulligan et al., (2019) where they compare experimental results with data by analytical models. In this study, the error amounts to up to 30% between models and experimental data.

Another difference in the results is the CFD study conducted in Ansys does not consider the conditions of the environment in which each study was carried out. This study only considers gravity and pressure in border conditions.

These results make it possible to determine that the proposed analytical models do not adequately characterize the vortex formed in the tank of this study, despite representing the same behavior between the walls and the air-core vortex.

5. CONCLUSION

In the present study, a CFD analysis was performed between two camera designs for a GVT, varying the geometry of the outlet hole (conical and cylindrical) while maintaining 14% of the camera aspect ratio. The study obtained the theoretical powers that can generate and tangential velocity profiles at different heights for each design, to compare the velocity profiles with higher tangential speed calculated by the analytical models.

Parameters such as geometry tank and the camera aspect ratio are some that influence the vortex formation directly. Conical geometry has an 11% higher tangential velocity than cylindrical them. It is due to the conical outlet geometry gives the flow a smooth transition, reducing losses from the configured case with cylindrical outlet. Additionally, for both geometries, the speed profiles in the camera tank increase significantly close to the air core and the discharge zone. Presenting a higher tangential velocity reduction of 40% between 0.1 and 0.3 m of radius for the conical geometry.

In addition to tangential velocity, the conical geometry exhibited a higher theoretical power generated at the three heights taken. Errors between powers range from 8 to 10% for the height of 0.050 and 0.200m, respectively. This result is a good help in determining the height to locate a rotor in case of extracting the kinetic energy from the water and transforming it into mechanical energy.

Thanks to the CFD study it can be demonstrated that the geometric design of the discharge zone directly affects the performance of a gravitational vortex turbine. Only by modifying the discharge zone and preserving the same operating conditions and the other geometric parameters of the tank (diameter, area

reduction, camera height, etc.) can increase theoretical in the tangential velocity of 11%.

6. AUTHORS' NOTE

The authors declare that there is no conflict of interest regarding the publication of this article. Authors confirmed that the paper was free of plagiarism.

7. REFERENCES

- Date, A., and Akbarzadeh, A. (2009). Design and cost analysis of low head simple reaction hydro turbine for remote area power supply. *Renewable Energy*, 34(2), 409-415.
- Dhakal, R., Bajracharya, T. R., Shakya, S. R., Kumal, B., Williamson, S., Khanal, K., Gautam, S., and Ghale, D. P. (2018). Computational and experimental investigation of runner for gravitational water vortex power plant. *2017 IEEE 6th International Conference on Renewable Energy Research and Applications (ICRERA 2017)*, 5(8), 365-373.
- Dhakal, S., Timilsina, A. B., Fuyal, D., and Ratna Bajracharya, T. (2014). Effect of dominant parameters for conical basin: Gravitational water vortex power plant. *Proceedings of IOE Graduate Conference*, 5, 381.
- Du, J., Shen, Z., and Yang, H. (2018). Effects of different block designs on the performance of inline cross-flow turbines in urban water mains. *Applied Energy*, 228, 97-107.
- Einstein, H. A., and Li, H. (2011). Le vortex permanent dans un fluide réel steady vortex flow in a real fluid. *La Houille Blanche*, 41(4), 483-496.
- Hite Jr, J. E., and Mih, W. C. (1994). Velocity of air-core vortices at hydraulic intakes. *Journal of Hydraulic Engineering*, 120(3), 284-297.
- Laaraba, A., and Khechekhouche, A. (2018). Numerical simulation of natural convection in the air gap of a vertical flat plat thermal solar collector with partitions attached to its glazing. *Indonesian Journal of Science and Technology*, 3(2), 95-104.
- Marian, G., Sajin, T., Florescu, I., Nedelcu, D. I., Ostahie, C. N., and Bîrsan, C. (2012). The concept and theoretical study of micro hydropower plant with gravitational vortex and turbine with rapidity steps. *Buletinul AGIR*, 3, 219-226.
- Márquez, J. L., Molina, M. G., and Pacas, J. M. (2010). Dynamic modeling, simulation and control design of an advanced micro-hydro power plant for distributed generation applications. *International Journal of Hydrogen Energy*, 35(11), 5772-5777.
- Mohamed, A. A. F. A. A. (2018). Hybrid nanocrystal photovoltaic/wind turbine power generation system in buildings. *Journal of Advanced Research in Materials Science*, 40(1), 8-19.
- Mulligan, S., Creedon, L., Casserly, J., and Sherlock, R. (2019). An improved model for the tangential velocity distribution in strong free-surface vortices: An experimental and theoretical study. *Journal of Hydraulic Research*, 57(4), 547-560.

- Odgaard, A. J. (1986). Free-surface air core vortex. *Journal of Hydraulic Engineering*, 112(7), 610-620.
- Rahman, M. M., Tan, J. H., Fadzlita, M. T., and Muzammil, A. W. K. (2017). A review on the development of gravitational water vortex power plant as alternative renewable energy resources. *IOP Conference Series: Materials Science and Engineering*, 217(1), 012007.
- Rehan, K., H. H., Y., and Pao, W. (2019). Numerical investigation of the elbow angle effect on solid particle erosion for liquid-solid flow. *International Journal of Mechanical and Mechatronics Engineering IJME-IJENS*, 19(1), 1–13.
- Rosenhead, L. (1930). The spread of vorticity in the wake behind a cylinder. *The Royal Society Publishing*, 127(806), 590–612.
- Shabara, H. M., Yaakob, O. B., Ahmed, Y. M., Elbatran, A. H., and Faddir, M. S. (2015). CFD validation for efficient gravitational vortex pool system. *Jurnal Teknologi*, 74(5), 97-100.
- Şibil, R., Aras, E., and Kankal, M. (2021). Comparison of various turbulence model performance in computational fluid dynamics analyses of the oxidation ditches with experimental validation. *Process Safety and Environmental Protection*, 154, 43-59.
- Vatistas, G. H., Lin, S., and Kwok, C. K. (1986). Theoretical and experimental studies on vortex chamber flows. *AIAA Journal*, 24(4), 635-642.
- Wanchat, S., and Suntivarakorn, R. (2012). Preliminary design of a vortex pool for electrical generation. *Advanced Science Letters*, 13(1), 173-177.
- Wanchat, S., Suntivarakorn, R., Wanchat, S., Tonmit, K., and Kayanyiem, P. (2013). A parametric study of a gravitation vortex power plant. *Advanced Materials Research*, 805, 811-817.
- Wichian, P., and Suntivarakorn, R. (2016). The effects of turbine baffle plates on the efficiency of water free vortex turbines. *Energy Procedia*, 100, 198-202.